







# Analysis of light diffraction by azobenzene-based photoalignment layers

ALEX BERDIN,<sup>1</sup>  JORDAN R. GILL,<sup>2</sup> ELENI PERIVOLARI,<sup>3</sup>  
JOEL KAUPPO,<sup>4</sup> VASILIS APOSTOLOPOULOS,<sup>3</sup>   
GIAMPAOLO D'ALESSANDRO,<sup>2,5</sup>  MALGOSIA KACZMAREK,<sup>3</sup>  
AND ARRI PRIIMAGI<sup>1,6</sup> 

<sup>1</sup>*Faculty of Engineering and Natural Sciences, Tampere University, FI-33720 Tampere, Finland*

<sup>2</sup>*School of Mathematical Sciences, University of Southampton, Southampton SO17 1BJ, UK*

<sup>3</sup>*School of Physics & Astronomy, University of Southampton, Southampton SO17 1BJ, UK*

<sup>4</sup>*Department of Applied Physics, Aalto University, FI-02150 Espoo, Finland*

<sup>5</sup>*dales@oton.ac.uk*

<sup>6</sup>*arri.priimagi@tuni.fi*

**Abstract:** Photoalignment materials, such as the azobenzene-based PAAD series studied here, are becoming increasingly important in liquid crystal-based optical devices and displays. Yet their properties and, in particular, their response to light, are still not fully understood. We investigate, experimentally and theoretically, the photoinduced birefringence, the order parameter and the formation of surface relief gratings, as well as the diffraction caused by them. We show that some of the azobenzene PAAD materials are suitable for the formation of surface relief gratings with high modulation depth, while others exhibit strong photoinduced birefringence. The two effects are inversely correlated: the stronger the surface relief grating is, the weaker is photoinduced birefringence. Analytical formulas based on the Raman-Nath approximation and numerical simulations of Maxwell's equations are used to quantify the diffraction caused by the induced diffraction gratings, showing excellent agreement between theory and experiment.

Published by Optica Publishing Group under the terms of the [Creative Commons Attribution 4.0 License](https://creativecommons.org/licenses/by/4.0/). Further distribution of this work must maintain attribution to the author(s) and the published article's title, journal citation, and DOI.

## 1. Introduction

Controlled surface-mediated alignment of anisotropic materials is the key element behind the operation of essentially all liquid crystal (LC) devices [1–3]. The most conventional LC alignment technique is mechanical rubbing of the surfaces of the LC cell with a suitable material such as velvet fabric, to induce nanoscopic grooves that anchor the LC molecules to the direction of the grooves [4–6]. The rubbing method is convenient and actively used in the liquid crystal display (LCD) industry, but the physical contact required renders the technique susceptible to defects arising from, e.g., debris and static charges. Moreover, rubbing cannot be applied within closed volumes, nor is it suitable for obtaining complex LC alignment patterns required, e.g., in diffractive waveplates [7]. These drawbacks can be addressed via photoalignment, in which thin photosensitive layers are used to control the LC alignment in response to irradiation with polarized light [8–11]. Photoalignment has huge potential in various photonic technologies [12,13]. At the same time, the process can be sensitive to environmental cues such as humidity [14]. To fully utilize the photoalignment technology, it is important to increase the library of available photoalignment materials and techniques [15,16], and to understand in detail the photoresponsive properties of those already available.

Among the wealth of photoalignment materials available, azobenzene-containing small molecules and polymers constitute an important class [17–20]. The underlying phenomenon

behind essentially all photoinduced effects in azobenzene-containing systems is the photochemical isomerization between the thermodynamically stable *trans* form and the metastable *cis* form under irradiation with UV or visible light, depending on the molecular structure [21,22]. From the perspective of LC photoalignment, the ability of azobenzene-containing thin films to undergo orientational redistribution in response to irradiation with polarized light [10,23] is particularly relevant. The net effect of prolonged illumination of such films is the preferential alignment of the long axes of the azobenzene molecules perpendicular to the polarization of incident light [24]. This preferential alignment is transmitted to the liquid crystals and has been used to create a wealth of dynamic photonic elements such as optical switches, polarization gratings and waveplates [25–31].

Many of the above-mentioned optical elements are obtained by periodic patterning of the photoalignment layer (and as a result, the molecular director of the LC) with laser interference patterns. However, the laser interference patterns are also known to invoke macroscopic mass migration into azobenzene-containing thin films, resulting in the formation of surface-relief gratings (SRGs) [32,33]. These temporally stable topographic structures can be hundreds of nanometers in modulation height and they can be superposed [34,35], erased [36,37], and rewritten [38], showing promise for applications in photonics and microfabrication [39,40]. There are also reports on SRGs dictating the alignment of LCs [41,42], but they have not been reported in the context of commonly used, commercially available photoalignment materials. While in some cases it can be beneficial to suppress the SRG formation [43], SRG-forming photoalignment layers could provide interesting perspectives towards synergistic use of SRGs and orientational redistribution in controlling the LC alignment. Prior to this, it would be important to understand whether (and under which conditions) SRGs form on the photoalignment layers, and to analyze the role of the SRG formation and the orientational redistribution in their overall diffraction signal [44–46].

Herein, we study the photoinduced birefringence, order parameter and SRG formation on different azobenzene-based PAAD photoalignment materials [47–49], proprietary materials provided to us by the manufacturer (BEAM Co., Orlando, FL) that are used in a wealth of applications ranging from transparent planar optics [30] to structurally colored [50] and photoactuable [51] liquid crystalline networks. We study PAAD layers of different thicknesses, from sub-100 nm to approximately 300 nm, and show that SRG formation indeed takes place. In some materials, such as PAAD-52, the SRG amplitude even exceeds the original film thickness. We also study the relationship between photoinduced anisotropy and the SRG formation efficiency, indicating that they are inversely correlated: the materials with efficient SRG formation tendency yield modest photoinduced anisotropy and vice versa. Finally, we perform an in depth analysis of the PAAD film diffraction efficiency. We verify the diffraction efficiency measurements by comparing them to predicted values based on the Raman-Nath model and on numerical simulations of Maxwell's equations.

## 2. Methods

PAAD films with thicknesses ranging from 90 to 270 nm were prepared by dissolving a series of commercially available photoalignment materials (PAAD-22B, PAAD-22C, PAAD-22D, PAAD-22E, PAAD-22N, PAAD-23W, PAAD-33W, PAAD-52 and PAAD-72) in dimethylformamide (DMF) with concentrations of typically 7 wt-%, depending somewhat on the solubility of the PAAD in question. The solutions were filtered twice through a 0.02  $\mu\text{m}$  PTFE membrane filter and spin-coated onto pre-cleaned glass substrates. The coatings were then heated to 80 °C to remove any residual solvent. The film thickness was determined using a stylus profilometer (Veeco Dektak). The quality of the coatings and the presence of crystallinity were evaluated by optical microscopy.

Photoinduced birefringence was measured by placing the sample between crossed polarizers and illuminating with a linearly polarized pump beam (488 nm, Ar<sup>+</sup>) at an intensity of approximately 100 mW/cm<sup>2</sup> to align the azobenzene units perpendicular to the polarization of the irradiation beam. A laser diode with an emission wavelength of 820 nm was used as the probe beam, which is outside the absorption spectrum of the samples. The polarizer and analyzer were aligned  $\pm 45^\circ$  with respect to the pump beam to maximize the transmitted signal. Birefringence was determined by measuring the temporal variation of the signal before, during and after irradiation with the pump beam. Absolute birefringence was calculated as a function of the transmitted signal using the following equation [52],

$$\Delta n = \frac{\lambda}{\pi d} \arcsin \left[ \left( \frac{I(t)}{I_0} \right)^{\frac{1}{2}} \right], \quad (1)$$

where  $I_0$  is the measured signal without sample and with parallel polarizers,  $d$  is the thickness of the film,  $\Delta n$  is the PAAD birefringence and  $\lambda$  is the wavelength of the probe beam. To erase the induced birefringence, the sample was illuminated with circularly polarized light by placing a quarter-wave plate between the pump beam and the sample.

Photoinduced dichroism was studied with an optical setup that consists of a linearly polarized pump beam, a white light probe beam (with low enough intensity not to isomerize the azobenzene molecules), and two fiber-optic spectrometers. The wavelength of the pump beam used was either 365 nm or 457 nm, depending on the wavelength of maximum absorbance of the studied material. The samples were irradiated with the pump beam until saturation. The probe beam passing through the sample was split into two beams by a beam splitter (BS). The absorbance of each beam was measured using spectrometers with polarizers (P), one parallel and the other perpendicular to the polarization of the pump beam, so that the parallel and perpendicular absorbances could be measured in real time. The order parameter is expressed as

$$S = \frac{|A_{\parallel} - A_{\perp}|}{A_{\parallel} + 2A_{\perp}}, \quad (2)$$

where  $A_{\parallel}$  and  $A_{\perp}$  is the absorbance parallel and perpendicular to the polarization of the activating light, respectively.

Surface-relief gratings were inscribed on the samples with circularly polarized light (yielding a polarization modulation pattern) using the Lloyd's mirror setup [53], where the interference pattern is created by coinciding two halves of an expanded laser beam (one impinging directly on the material surface and the other reflecting from the mirror) on the sample surface. The setup uses a 488 nm argon laser beam for irradiation at an intensity of 250 mW/cm<sup>2</sup>. The periodicity of the surface relief grating can be expressed as

$$\Lambda = \frac{\lambda}{2 \sin(\theta)}, \quad (3)$$

where  $\Lambda$  is the resulting grating period,  $\lambda$  is the wavelength of the laser beam, and  $\theta$  is the angle between the incident beam and the sample normal. Thus, the periodicity can be easily varied by changing the angle  $\theta$ . All the diffraction efficiency data reported here used gratings with  $\Lambda = 1 \mu\text{m}$ . A p-polarized probe beam from a HeNe laser at a wavelength of 632.8 nm was used to measure the diffraction efficiency over time by monitoring the first diffraction order with a power meter. The diffraction efficiency was calculated using the ratio between the power of the first diffraction versus the power of the incident beam.

### 3. Results and discussion

Depending on the PAAD in question, the photoalignment layers absorb from UV all the way to yellow wavelengths, providing the possibility to use a wide range of light sources (the absorption

spectra of PAAD-22 and PAAD-72 are given as examples in Fig. 1(a), as they are the more easily available PAAD materials). Irradiation with linearly polarized light within the absorption band induces photoisomerization of the azobenzene moieties and resultant alignment of the chromophores perpendicular to the polarization of the incident light, giving rise to birefringence and dichroism. The obtained birefringence varied greatly between the studied PAAD materials. For example, for PAAD-22 birefringence of  $\Delta n \approx 0.18$  was measured, while for PAAD-72 the value was only  $\Delta n \approx 0.04$  (Fig. 1(b)). In fact, relatively high birefringence was achieved only for PAAD-22 and PAAD-22B (0.18 and 0.13, respectively), whereas most of the samples showed  $\Delta n$  values below 0.1. This result is in agreement with our earlier work [49]. The low birefringence values of PAAD 22D, E and N were indirectly obtained from diffraction efficiency measurements from their very thin, spin-coated films, namely 20 to 70 nm [49] with  $\Delta n$  varying between 0.001-0.05. For all materials, the birefringence could be erased using circularly polarized light (Fig. 1(b)).

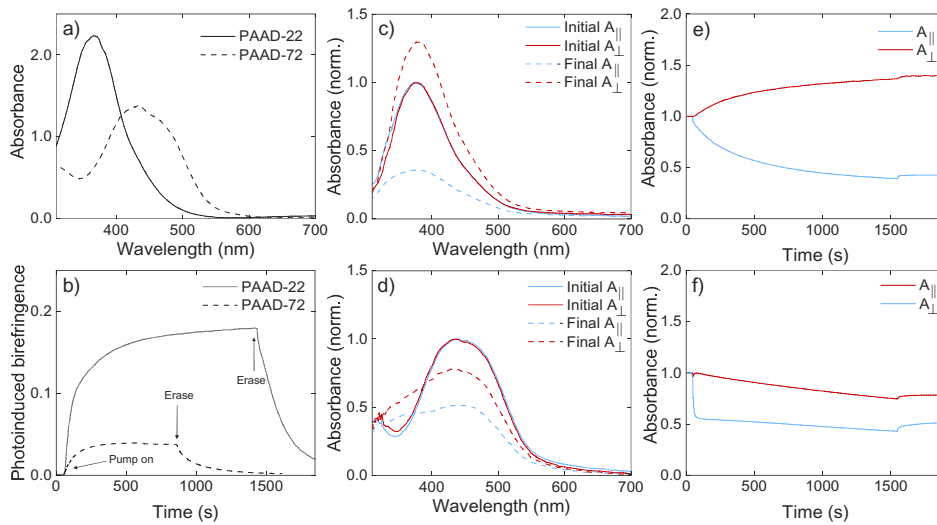


**Fig. 1.** The absorption spectra (a) and photoinduced birefringence curves (b) for PAAD-22 and PAAD-72. The birefringence is inscribed with linearly polarized and erased with circularly polarized laser beam. Polarized absorption spectra before and after irradiation for PAAD-22 (c) and PAAD-72 (d).  $A_{\parallel}$  and  $A_{\perp}$  denote the absorbances parallel and perpendicular to the polarization of the excitation beam. The time dynamics of the photoinduced dichroism at  $\lambda_{max} = 372$  nm for PAAD-22 (e) and at  $\lambda_{max} = 433$  nm for PAAD-72 (f).

Figure 1(c) and 1(d) show the polarized absorption spectra for PAAD-22 and PAAD-72, respectively, before and after irradiation (20 min of irradiation, followed by 5 min of relaxation). Figure 1(e) and 1(f) show the dynamics of the corresponding absorption changes at the maximum absorption wavelength,  $\lambda_{max}$ . For PAAD-22, the absorbance parallel to the pump polarization decreases and the one in the perpendicular direction increases, confirming that the molecules indeed photoalign perpendicular to the polarization of the pump light. The order parameter calculated from Eq. (2) is  $S \approx 0.32$ , measured at  $\lambda_{max} = 366$  nm (Fig. 1(e)). As a comparison, the order parameter for SD-1, another widely used commercially available photoalignment material, is  $S \approx 0.4$  at  $\lambda_{max} = 372$  nm [54]. For PAAD-72, the behavior is different, and it can be seen that the absorbance in both parallel and perpendicular directions decreases upon light irradiation, yielding  $S \approx 0.13$  at  $\lambda_{max} = 433$  nm (Fig. 1(f)). While the exact cause for this difference is unknown, it most likely relates to differences in the cis–trans isomerization dynamics between the two materials and the photostationary state population, which is expected to be more cis-rich for

PAAD-72 [55,56] due to stronger absorption at the excitation wavelength (488 nm). Nevertheless, in both materials the photoinduced anisotropy is reversible (Fig. 1(b)), and both act as efficient photoaligning materials for LCs [57,58]. Hence, high birefringence/order parameter does not seem to be a prerequisite for efficient LC photoalignment. The birefringence and order parameter values for all the materials studied are given in Table 1.

**Table 1. Experimental measurements of different PAAD films**

PAAD	Thickness (nm)	Birefringence	Order param.	Modulation (nm)	Diff. eff.
22	240	0.18	0.32	0	1.7%
23W	90	0.035	0.13	15	0.6%
22B	210	0.125	0.23	18	0.8%
22C	220	0.002	0.09	38	0.7%
22N	250	0.068	0.06	42	0.9%
22D	100	0.002	0.07	54	0.8%
52	100	0.006	0.05	115	4.2%
22E	120	0.002	0.09	115	3.8%
22D	215	0.002	0.07	140	6.2%
72	270	0.04	0.13	140	5.7%
33W	140	0	0.07	160	8.8%
52	225	0.006	0.05	325	27.2%

We next proceeded to study the SRG formation in the PAAD films under interference illumination. The used circularly polarized illumination in the Lloyd mirror geometry yielded a polarization modulation pattern with only minor modulation in the illumination intensity [53]. Our main observation is that for the majority of the samples the SRG formation indeed took place. Using again PAAD-22 and PAAD-72 as examples, the diffraction signal for both under interference illumination is shown in Fig. 2(a). For PAAD-72, the diffraction efficiency gradually increased and saturated after ca. 20 min exposure to a value between 5 and 6%. For PAAD-22 the diffraction dynamics was very different, and the diffraction efficiency instantaneously jumped to ca. 1.5% and did not change under prolonged irradiation. Clearly the origin of diffraction is different in the two cases. We also studied the polarization dependence of the SRG formation for PAAD-72. From Fig. 2(b) it can be seen that circular polarization resulted in the most efficient SRG formation. p-polarization yielded comparable, yet somewhat weaker diffraction efficiency, while the diffraction in response to s-polarized pump beam was negligible. This is in line with observations from many other azobenzene-based systems. [59,60]. For PAAD-72, AFM characterization confirmed that an SRG was indeed formed. Figure 2(c) shows the final topography of the inscribed grating after illumination. From the surface profile in Fig. 2(d), the modulation depth was determined to be 140 nm, with a periodicity around 1  $\mu\text{m}$ . For PAAD-22, in turn, no SRG was formed. Instead, the diffraction arises from efficient photoalignment, yielding a bulk birefringence grating at the periodicity dictated by the light interference pattern [44,61]. Hence the material that could be efficiently photoaligned (PAAD-22) yielded no SRG while the one with low photoinduced birefringence (PAAD-72) exhibited efficient SRG formation.

Comparing SRG formation and photoinduced birefringence in various PAAD materials, it can be seen more generally that these two processes seem to be negatively correlated to each other. This observation is summarized in Table 1, which shows that PAAD-52, which is by far the most efficient SRG-forming material, yields negligible birefringence and photoinduced order parameter of only 0.05, while on the other end of the spectrum, PAAD-22 does not undergo SRG formation but yields an order parameter exceeding 0.3. This trend is further highlighted in Fig. 3, based on which we divide the PAAD materials in two classes – those with high birefringence (e.g.

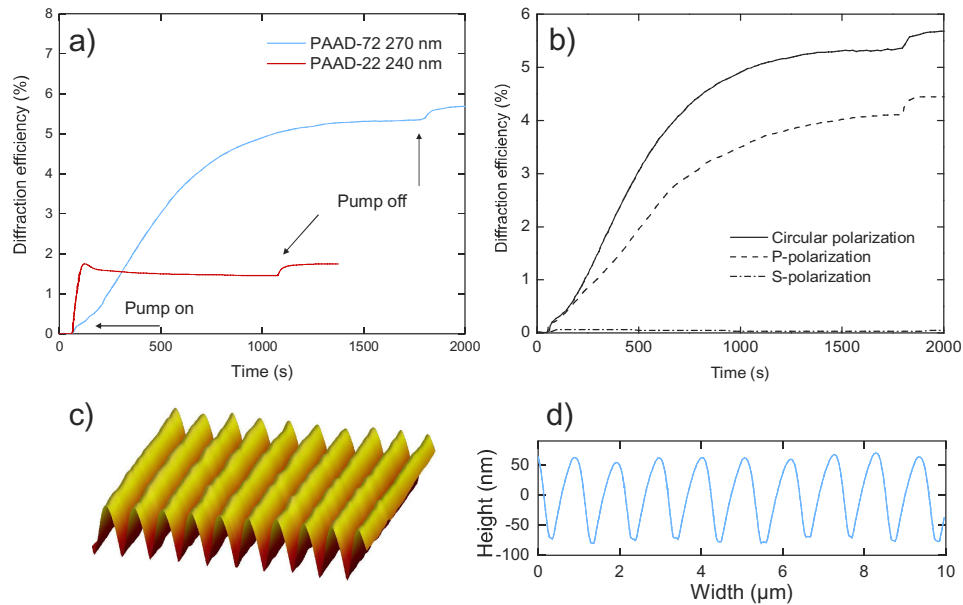


**Fig. 2.** (a) Measured diffraction efficiency as a function of pump illumination time for PAAD-22 and PAAD-72. (b) Measured diffraction efficiency from PAAD-72 for differently polarized pump beam. (c) Surface topography from AFM measurements of a surface-relief grating inscribed on a 270 nm thick PAAD-72 film with an interference pattern of a circularly polarized 488 nm laser beam of intensity  $255 \text{ mW/cm}^2$ . (d) Cross section of the surface topography.

PAAD-22), exhibiting “conventional” photoalignment, and those that are good for SRG formation (e.g. PAAD-52, PAAD-33W), the modulation depth even exceeding the original film thickness.

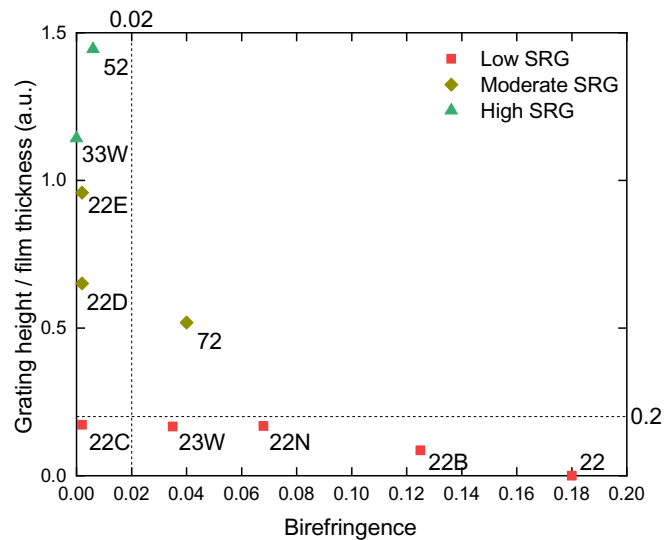


**Fig. 3.** Comparison of surface relief grating formation and photoinduced birefringence in the PAAD materials studied. Both processes are negatively correlated.

An interesting combination between the two extremes is PAAD-72. It forms gratings with moderate height and at the same time, exhibits modest photoinduced birefringence/dichroism. We believe that PAAD-72 has the potential to combine both properties and can therefore be used in the future to study the competing effects of topography and photoalignment in LC-based optical elements [62].

#### 4. Modeling the diffraction efficiency

We have modeled the diffraction efficiency of the surface relief gratings using a Raman-Nath approximation [63] to get an approximate analytical relation between the experimental parameters and the diffraction efficiency values. We have verified the accuracy of the approximation by comparing it to numerical solutions of the full Maxwell equations.

We represent the PAAD film as a layer with one flat boundary adjacent to the glass substrate and a sinusoidal boundary in contact with air. The film thickness  $L$  is assumed to be

$$L = L_0 + \Delta L \sin\left(2\pi \frac{x}{\Lambda}\right), \quad (4)$$

where  $L_0$  is the average film thickness and  $\Delta L$  the amplitude of the sinusoidal modulation. The coordinate system is chosen so that the  $x$ -axis is parallel the grating wave vector and the  $z$ -axis is perpendicular to the glass-PAAD boundary (see Fig. 4).

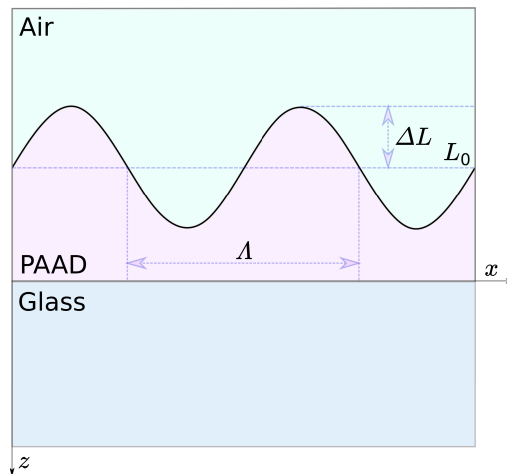


**Fig. 4.** Schematic diagram of the PAAD film for the purpose of computing its diffraction efficiency.

The Raman-Nath approximation neglects diffraction during propagation across the film and also polarization dependent effects. These are reasonable approximations, the former because the film thickness is smaller than the light wavelength, the latter because the film anisotropy is relatively weak. We can justify this last statement by noting that there are two sources of anisotropy in the film optical response. The first is the intrinsic birefringence of the PAAD material. However, as can be seen from Table 1, this is in general relatively small with respect to the PAAD to air refractive index contrast. The second is the polarization dependence of the Fresnel transmission and reflection formulae. As we are only considering diffraction from normal incidence beams, the maximum angle between direction of propagation and PAAD-air boundary is  $\pi/4$ , a range where the polarization effect in the Fresnel formulae is relatively modest and hence can be considered only a small correction.

The optical path length for a beam at normal incidence propagating through the film is (see Fig. 4)

$$\delta_{\text{opt}} = L' + \Delta L(n_p - 1) \sin\left(2\pi \frac{x}{\Lambda}\right), \quad (5)$$

where  $L' = n_p L_0 + \Delta L$  and  $n_p$  is the PAAD (isotropic) refractive index. The refractive index of air is assumed to be 1.

In the Raman-Nath approximation the only effect of the grating is to modulate the phase of the incoming linearly polarized beam so that the electric field immediately after the grating can be written as

$$E = E_0 e^{i(kz - \omega t)} e^{i\Phi} e^{i\delta \sin(2\pi \frac{x}{\Lambda})}, \quad (6)$$

where  $k$  is the wave number in air,  $\omega$  the angular frequency,  $\Phi$  a global constant phase factor and  $\delta = 2\pi \Delta L(n_p - 1)/\lambda$ . We use the Jacobi-Anger identity for Bessel functions,

$$e^{i\delta \sin(x)} = \sum_{m=-\infty}^{+\infty} J_m(\delta) e^{imx}, \quad (7)$$

where  $J_m$  are the Bessel function of first kind of order  $m$ , to write the field immediately after the grating as a linear superposition of plane waves, the diffracted orders, [64]

$$E = E_0 e^{i(kz - \omega t)} e^{i\Phi} \sum_{m=-\infty}^{+\infty} J_m(\delta) e^{im2\pi x/\Lambda}. \quad (8)$$

The intensity of the  $m$ -th diffracted order is  $|E_0|^2 J_m^2(\delta)$ . In non-paraxial Raman-Nath theory, one can show that the first order diffraction efficiency,  $\eta_{RN}$ , is given by [65, Eq. (31)]

$$\eta_{RN} = \frac{J_1^2(\delta)}{\max \sum_{m=\min} J_m^2(\delta)}, \quad (9)$$

where the sum in the denominator is restricted to the forward propagating diffracted orders. For  $\lambda = 632$  nm and  $\Lambda = 1$   $\mu\text{m}$  at normal incidence only the waves with  $m = 0$  and  $m = \pm 1$  are non-evanescent so that the diffraction efficiency in the Raman-Nath approximation is

$$\eta_{RN} = \frac{J_1^2(\delta)}{J_0^2(\delta) + 2J_1^2(\delta)}. \quad (10)$$

To test the validity of the Raman-Nath approximation, we have also solved the full Maxwell equations numerically using COMSOL. We have used the ‘‘Electromagnetic Waves, Frequency Domain’’ Physics Module to simulate the propagation of a monochromatic wave through an isotropic layered structure comprising an air layer, a PAAD layer with one side flat and one side sinusoidal, and a glass layer. The entire structure was sandwiched between two perfectly matched layers to simulate waves propagating from and to infinity. The diffraction efficiency was computed using a port condition on the outward side of the glass layer.

The results of the two approaches and their agreement with the experimental data for surface relief gratings summarized in Table 1 is reported in Fig. 5. In estimating the diffraction efficiency we have assumed that the refractive indices of the different PAAD variants are similar. We have assumed that the refractive index is  $n_p = 1.73$ , as fitted from thin PAAD film experimental data [66] using the Iterated Ray Method [67]. A comparison between the curves shows that, even though the effect of diffraction and polarization become more significant for thicker gratings, the Raman-Nath diffraction formula (10) is a valid approximation. A second observation that can be



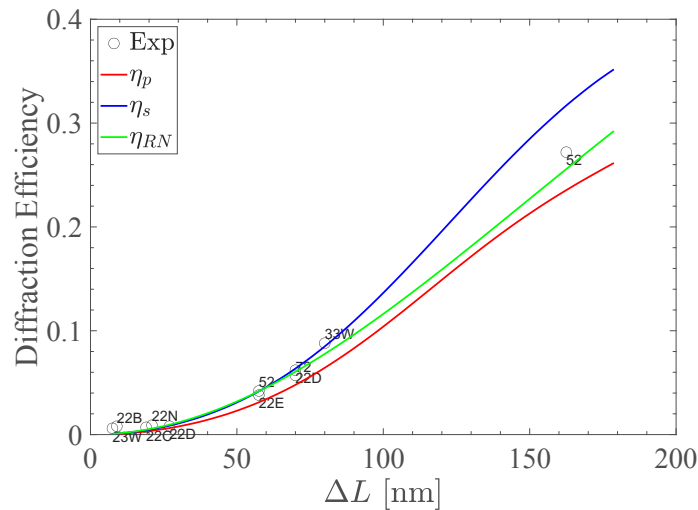


**Fig. 5.** Diffraction efficiency of surface relief gratings - The experimental data in Table 1 is represented by the open circles with the PAAD type written next to them. The curves represent the theoretical diffraction efficiency for a grating with refractive index  $n_p = 1.73$  computed using the isotropic Raman-Nath formula (10),  $\eta_{RN}$ , and a Comsol simulation of the full Maxwell equations for an s- and p-polarizes probe beam,  $\eta_s$  and  $\eta_p$  respectively.

made from these data is that the scattering of the probe is stronger for the s-polarization in the case of surface relief gratings.

These results are consistent with diffraction efficiency measurements in very thin PAAD films, measured in separate experiments. Short time (15 s) and low power (10 mW  $\text{Ar}^+$  laser at 514.5 nm) illumination of thin (20-30 nm) spin-coated PAAD-22E films produced no surface gratings and a very small diffraction efficiency, approximately  $10^{-6}$ , attributed to a polarization grating [49]. In more recent experiment, longer (15 minutes) exposure times with larger power (300 mW) in PAAD films of the same thickness gave a diffraction efficiency that was two orders of magnitude larger [66]. The work on such system is still ongoing, but these preliminary results indicate that longer exposure and higher intensity can lead to the formation of surface relief grating even in very thin films. The analysis based on Eq. (10) suggests that a modulation of approximately 5 nm of the 20-30 nm thick film would have produced the required effect.

## 5. Conclusion

We have investigated the surface relief grating formation in commercially available, azobenzene-based photoalignment materials (PAAD, BEAM Co.). The SRG formation was indeed experimentally confirmed, and modelled using Raman-Nath approximation. The best-performing SRG-forming material, PAAD-52, yielded diffraction efficiency of 27% and grating modulation depth notably higher than the film thickness. The SRG formation and photoinduced birefringence/dichroism were found to be negatively correlated, with PAAD-22 having the highest birefringence (0.18) and PAAD-52 the highest grating amplitude (325 nm). We point out PAAD-72 as a particularly interesting material, combining both reasonably high photoinduced anisotropy and SRG modulation height. These two effects, possibly combined with the repeatability of erasure properties of PAAD [68], may in the future be potentially used as independent control parameters for controlling LC alignment and anchoring energy on the PAAD layers, opening new possibilities for real-time-tunable liquid crystal-based optical elements.

**Funding.** Engineering and Physical Sciences Research Council (ES/T502029/1); Academy of Finland PREIN Flagship

Programme, No. 320165 and P-Cap project No.324353.

**Acknowledgments.** We gratefully acknowledge Nelson Tabiryan from BEAM Co. for providing the photoalignment materials and Marina Grenzer–Saphiannikova (Institute Theory of Polymers, Dresden) for helpful discussions on modeling azobenzene based materials.

**Disclosures.** The authors declare no conflicts of interest.

**Data availability.** Data will be made available upon reasonable request.

## References

1. M. Schadt, H. Seiberle, and A. Schuster, "Optical patterning of multi-domain liquid-crystal displays with wide viewing angles," *Nature* **381**(6579), 212–215 (1996).
2. H. Coles and S. Morris, "Liquid-crystal lasers," *Nat. Photonics* **4**(10), 676–685 (2010).
3. J. Beeckman, K. Neyts, and P. J. M. Vanbrabant, "Liquid-crystal photonic applications," *Opt. Eng.* **50**(8), 081202 (2011).
4. A. A. Sonin, *The surface physics of liquid crystals* (Taylor & Francis, 1995).
5. J. Stöhr and M. Samant, "Liquid crystal alignment by rubbed polymer surfaces: a microscopic bond orientation model," *J. Electron Spectrosc. Relat. Phenom.* **98-99**, 189–207 (1999).
6. S. Ishihara and M. Mizusaki, "Alignment control technology of liquid crystal molecules," *J. Soc. Inf. Disp.* **28**(1), 44–74 (2020).
7. S. R. Nersisyan, N. V. Tabiryan, D. M. Steeves, and B. R. Kimball, "The promise of diffractive waveplates," *Opt. Photonics News* **21**(3), 40–45 (2010).
8. W. M. Gibbons, P. J. Shannon, S.-T. Sun, and B. J. Swetlin, "Surface-mediated alignment of nematic liquid crystals with polarized laser light," *Nature* **351**(6321), 49–50 (1991).
9. A. G. Dyadyusha, V. M. Kozenkov, T. Y. Marusiy, Y. A. Reznikov, V. Y. Reshetnyak, and A. Khizhnyak, "Light-induced planar alignment of nematic liquid-crystal by the anisotropic surface without mechanical texture," *Ukrainskii Fizicheskii Zhurnal* **36**, 1059–1062 (1991).
10. K. Ichimura, "Photoalignment of liquid-crystal systems," *Chem. Rev.* **100**(5), 1847–1874 (2000). PMID: 11777423.
11. T. Seki, "New strategies and implications for the photoalignment of liquid crystalline polymers," *Polym. J.* **46**(11), 751–768 (2014).
12. O. Yaroshchuk and Y. Reznikov, "Photoalignment of liquid crystals: basics and current trends," *J. Mater. Chem.* **22**(2), 286–300 (2012).
13. V. Chigrinov, J. Sun, and X. Wang, "Photoaligning and Photopatterning: New LC Technology," *Crystals* **10**(4), 323 (2020).
14. Y. Shi, C. Zhao, J. Y.-L. Ho, V. V. Vashchenko, A. K. Srivastava, V. G. Chigrinov, H.-S. Kwok, F. Song, and D. Luo, "Exotic Property of Azobenzenesulfonic Photoalignment Material Based on Relative Humidity," *Langmuir* **33**(16), 3968–3974 (2017).
15. K. Fukuhara, S. Nagano, M. Hara, and T. Seki, "Free-surface molecular command systems for photoalignment of liquid crystalline materials," *Nat. Commun.* **5**(1), 3320 (2014).
16. K. Hisano, M. Aizawa, M. Ishizu, Y. Kurata, W. Nakano, N. Akamatsu, C. J. Barrett, and A. Shishido, "Scanning wave photopolymerization enables dye-free alignment patterning of liquid crystals," *Sci. Adv.* **3**(11), e1701610 (2017).
17. K. Ichimura, Y. Suzuki, T. Seki, A. Hosoki, and K. Aoki, "Reversible change in alignment mode of nematic liquid crystals regulated photochemically by command surfaces modified with an azobenzene monolayer," *Langmuir* **4**(5), 1214–1216 (1988).
18. V. Chigrinov, A. Muravski, H. S. Kwok, H. Takada, H. Akiyama, and H. Takatsu, "Anchoring properties of photoaligned azo-dye materials," *Phys. Rev. E* **68**(6), 061702 (2003).
19. H.-S. Kwok, V. Chigrinov, H. Takada, and H. Takatsu, "New developments in liquid crystal photo-aligning by azo-dyes," *J. Displ. Technol.* **1**(1), 41–50 (2005).
20. N. Tsutsumi, "Recent advances in photorefractive and photoactive polymers for holographic applications," *Polym. Int.* **66**(2), 167–174 (2017).
21. H. M. D. Bandara and S. C. Burdette, "Photoisomerization in different classes of azobenzene," *Chem. Soc. Rev.* **41**(5), 1809–1825 (2012).
22. Z. Mahimwalla, K. G. Yager, J.-i. Mamiya, A. Shishido, A. Priimagi, and C. J. Barrett, "Azobenzene photomechanics: prospects and potential applications," *Polym. Bull.* **69**(8), 967–1006 (2012).
23. A. Natansohn and P. Rochon, "Photoinduced Motions in Azo-Containing Polymers," *Chem. Rev.* **102**(11), 4139–4176 (2002).
24. M. L. Dumont, S. Hosotte, G. Froc, and Z. Sekkat, "Orientational manipulation of chromophores through photoisomerization," in *Photopolymers and Applications in Holography, Optical Data Storage, Optical Sensors, and Interconnects*, R. A. Lessard, ed. (SPIE-Intl Soc Optical Eng, 1994).
25. L. De Sio, N. Tabiryan, T. Bunning, B. Kimball, and C. Umetsu, "Dynamic photonic materials based on liquid crystals," *Prog. Opt.* **58**, 1–64 (2013).

26. B. R. Kimball, D. M. Steeves, L. Hoke, N. V. Tabiryan, S. V. Serak, and U. A. Hrozhyk, "Azobenzene liquid crystalline materials for efficient optical switching with pulsed and/or continuous wave laser beams," *Opt. Express* **18**(8), 8697–8704 (2010).
27. L. Frey, M. Kaczmarek, J. M. Jonathan, and G. Roosen, "Analysis of gratings induced in azo-dye doped liquid crystals," *Opt. Mater.* **18**(1), 91–94 (2001).
28. S. R. Nersisyan, N. V. Tabiryan, D. Mawet, and E. Serabyn, "Improving vector vortex waveplates for high-contrast coronagraphy," *Opt. Express* **21**(7), 8205 (2013).
29. L. D. Sio, D. E. Roberts, Z. Liao, S. Nersisyan, O. Uskova, L. Wickboldt, N. Tabiryan, D. M. Steeves, and B. R. Kimball, "Digital polarization holography advancing geometrical phase optics," *Opt. Express* **24**(16), 18297 (2016).
30. N. V. Tabiryan, D. E. Roberts, Z. Liao, J.-Y. Hwang, M. Moran, O. Ouskova, A. Pshenichnyi, J. Sigley, A. Tabiryan, R. Vergara, L. De Sio, B. R. Kimball, D. M. Steeves, J. Slagle, M. E. McConney, and T. J. Bunning, "Advances in transparent planar optics: Enabling large aperture, ultrathin lenses," *Adv. Opt. Mater.* **9**(5), 2001692 (2021).
31. N. V. Tabiryan, D. Roberts, Z. Liao, E. Ouskova, J. Sigley, A. Tabiryan, J. Slagle, M. McConney, and T. J. Bunning, "Size, weight, and power breakthrough in nonmechanical beam and line-of-sight steering with geo-phase optics," *Appl. Opt.* **60**(25), G154 (2021).
32. P. Rochon, E. Batalla, and A. Natansohn, "Optically induced surface gratings on azoaromatic polymer films," *Appl. Phys. Lett.* **66**(2), 136–138 (1995).
33. D. Y. Kim, S. K. Tripathy, L. Li, and J. Kumar, "Laser-induced holographic surface relief gratings on nonlinear optical polymer films," *Appl. Phys. Lett.* **66**(10), 1166–1168 (1995).
34. M. Salvatore, F. Borbone, and S. L. Oscurato, "Deterministic Realization of Quasicrystal Surface Relief Gratings on Thin Azopolymer Films," *Adv. Mater. Interfaces* **7**(11), 1902118 (2020).
35. H. Rekola, A. Berdin, C. Fedele, M. Virkki, and A. Priimagi, "Digital holographic microscopy for real-time observation of surface-relief grating formation on azobenzene-containing films," *Sci. Rep.* **10**(1), 19642 (2020).
36. J. Jelken and S. Santer, "Light induced reversible structuring of photosensitive polymer films," *RSC Adv.* **9**(35), 20295–20305 (2019).
37. F. Lagugné Labarthe, T. Buffeteau, and C. Sourisseau, "Optical erasures and unusual surface reliefs of holographic gratings inscribed on thin films of an azobenzene functionalized polymer," *Phys. Chem. Chem. Phys.* **4**(16), 4020–4029 (2002).
38. T. Ubukata, T. Ioshima, and M. Hara, "Wavelength-Programmable Organic Distributed-Feedback Laser Based on a Photoassisted Polymer-Migration System," *Adv. Mater.* **17**(13), 1630–1633 (2005).
39. A. Priimagi and A. Shevchenko, "Azopolymer-based micro- and nanopatterning for photonic applications," *J. Polym. Sci. Part B: Polym. Phys.* **52**(3), 163–182 (2014).
40. K. Kim, H. Park, K. J. Park, S. H. Park, H. H. Kim, and S. Lee, "Light-Directed Soft Mass Migration for Micro/Nanophotonics," *Adv. Opt. Mater.* **7**(16), 1900074 (2019).
41. M.-H. Kim, J.-D. Kim, T. Fukuda, and H. Matsuda, "Alignment control of liquid crystals on surface relief gratings," *Liq. Cryst.* **27**(12), 1633–1640 (2000).
42. A. Madani, H. Khoshshima, H. Tajalli, and S. Ahmadi, "Experimental study of liquid-crystal alignment on a surface relief grating," *Laser Phys.* **16**(8), 1197–1201 (2006).
43. F. You, M. Paik, M. Häckel, L. Kador, D. Kropp, H.-W. Schmidt, and C. Ober, "Control and suppression of surface relief gratings in liquid-crystalline perfluoroalkyl–azobenzene polymers," *Adv. Funct. Mater.* **16**(12), 1577–1581 (2006).
44. F. Lagugné Labarthe, T. Buffeteau, and C. Sourisseau, "Analyses of the diffraction efficiencies, birefringence, and surface relief gratings on azobenzene-containing polymer films," *J. Phys. Chem. B* **102**(15), 2654–2662 (1998).
45. F. Lagugné Labarthe, T. Buffeteau, and C. Sourisseau, "Azopolymer holographic diffraction gratings: time dependent analyses of the diffraction efficiency, birefringence, and surface modulation induced by two linearly polarized interfering beams," *J. Phys. Chem. B* **103**(32), 6690–6699 (1999).
46. A. Sobolewska and A. Miniewicz, "Analysis of the Kinetics of Diffraction Efficiency during the Holographic Grating Recording in Azobenzene Functionalized Polymers," *J. Phys. Chem. B* **111**(7), 1536–1544 (2007).
47. U. Hrozhyk, S. Serak, N. Tabiryan, L. Hoke, D. M. Steeves, G. Kedziora, and B. Kimball, "High optical nonlinearity of azobenzene liquid crystals for short laser pulses," in *Liquid Crystals XII*, I. C. Khoo, ed. (SPIE, 2008).
48. S. R. Nersisyan, N. V. Tabiryan, D. M. Steeves, B. R. Kimball, V. G. Chigrinov, and H. S. Kwok, "Study of azo dye surface command photoalignment material for photonics applications," *Appl. Opt.* **49**(10), 1720–1727 (2010).
49. E. Mavrona, S. Mailis, N. Podoliak, G. D'Alessandro, N. Tabiryan, M. Trapatseli, J.-F. Blach, M. Kaczmarek, and V. Apostolopoulos, "Intrinsic and photo-induced properties of high refractive index azobenzene based thin films [invited]," *Opt. Mater. Express* **8**(2), 420 (2018).
50. K. R. Schlafmann and T. J. White, "Retention and deformation of the blue phases in liquid crystalline elastomers," *Nat. Commun.* **12**(1), 4916 (2021).
51. H. Zeng, O. M. Wani, P. Wasylczyk, R. Kaczmarek, and A. Priimagi, "Biomimetic materials: Self-regulating iris based on light-actuated liquid crystal elastomer (adv. mater. 30/2017)," *Adv. Mater.* **29**(30), 1 (2017).
52. D. Choi and S. Kang, "Dynamic behavior of photoinduced birefringence of copolymers containing aminonitro azobenzene chromophore in the side chain," *Bull. Korean Chem. Soc.* **20**(10), 1186–1194 (1999).

53. F. Lagugné-Labarthe, T. Buffeteau, and C. Sourisseau, "Inscription of holographic gratings using circularly polarized light: influence of the optical set-up on the birefringence and surface relief grating properties," *Appl. Phys. B: Lasers Opt.* **74**(2), 129–137 (2002).
54. H. Akiyama, T. Kawara, H. Takada, H. Takatsu, V. Chigrinov, E. Prudnikova, V. Kozenkov, and H. Kwok, "Synthesis and properties of azo dye aligning layers for liquid crystal cells," *Liq. Cryst.* **29**(10), 1321–1327 (2002).
55. P.-A. Blanche, P. C. Lemaire, M. Dumont, and M. Fischer, "Photoinduced orientation of azo dye in various polymer matrices," *Opt. Lett.* **24**(19), 1349–1351 (1999).
56. Z. Sekkat, D. Yasumatsu, and S. Kawata, "Pure photoorientation of azo dye in polyurethanes and quantification of orientation of spectrally overlapping isomers," *J. Phys. Chem. B* **106**(48), 12407–12417 (2002).
57. Y. Guo, M. Jiang, C. Peng, K. Sun, O. Yaroshchuk, O. Lavrentovich, and Q.-H. Wei, "High-resolution and high-throughput plasmonic photopatterning of complex molecular orientations in liquid crystals," *Adv. Mater.* **28**(12), 2353–2358 (2016).
58. G. Palermo, U. Cataldi, L. De Sio, T. Bürgi, N. Tabiryan, and C. Umeton, "Optical control of plasmonic heating effects using reversible photo-alignment of nematic liquid crystals," *Appl. Phys. Lett.* **109**(19), 191906 (2016).
59. X. L. Jiang, L. Li, J. Kumar, D. Y. Kim, V. Shivshankar, and S. K. Tripathy, "Polarization dependent recordings of surface relief gratings on azobenzene containing polymer films," *Appl. Phys. Lett.* **68**(19), 2618–2620 (1996).
60. F. Fabbri, D. Garrot, K. Lahlil, J. P. Boilot, Y. Lassailly, and J. Peretti, "Evidence of two distinct mechanisms driving photoinduced matter motion in thin films containing azobenzene derivatives," *J. Phys. Chem. B* **115**(6), 1363–1367 (2011). PMID: 21250737.
61. A. Sobolewska, S. Bartkiewicz, A. Miniewicz, and E. Schab-Balcerzak, "Polarization dependence of holographic grating recording in azobenzene-functionalized polymers monitored by visible and infrared light," *J. Phys. Chem. B* **114**(30), 9751–9760 (2010). PMID: 20666518.
62. D.-H. Chung, T. Fukuda, Y. Takanishi, K. Ishikawa, H. Matsuda, H. Takezoe, and M. A. Osipov, "Competitive effects of grooves and photoalignment on nematic liquid-crystal alignment using azobenzene polymer," *J. Appl. Phys.* **92**(4), 1841–1844 (2002).
63. C. Raman and N. N. Nath, "The diffraction of light by high frequency sound waves: Part ii," *Proc. - Indian Acad. Sci., Sect. A* **2**(4), 413–420 (1935).
64. R. Magnusson and T. K. Gaylord, "Diffraction efficiencies of thin phase gratings with arbitrary grating shape," *J. Opt. Soc. Am.* **68**(6), 806 (1978).
65. J. E. Harvey, A. Krywonos, and D. Bogunovic, "Nonparaxial scalar treatment of sinusoidal phase gratings," *J. Opt. Soc. Am. A* **23**(4), 858 (2006).
66. E. Perivolari, "Liquid crystal and meta-surface devices for enhancing light manipulation from visible to thz regime," Ph.D. thesis, School of Physics and Astronomy, University of Southampton (2022).
67. J. R. Gill, E. Perivolari, M. Kaczmarek, and G. D'Alessandro, "Efficient scattering model of multilayer systems with anisotropic films," *J. Opt. Soc. Am. A* **38**(5), 595 (2021).
68. E. Perivolari, J. Gill, N. Podoliak, V. Apostolopoulos, T. Sluckin, G. D'Alessandro, and M. Kaczmarek, "Optically controlled bistable waveplates," *J. Mol. Liq.* **267**, 484–489 (2018).